# Radio-frequency spectroscopy in the dark

W. Chalupczak,[1] P. Josephs-Franks,[1] R. M. Godun,[1] and S. Pustelny[2,3]
[1]*National Physical Laboratory, Hampton Road, Teddington, TW11 0LW, United Kingdom*
[2]*Institute of Physics, Jagiellonian University, Reymonta 4, PL 30-059 Kraków, Poland*
[3]*Department of Physics, University of California at Berkeley, Berkeley, California 94720-7300, USA*
(Received 3 September 2013; published 13 November 2013)

We demonstrate a technique for investigation of a strongly perturbed atomic system, which is an extension of standard radio-frequency spectroscopy. Analogous to "relaxation in the dark" experiments, this technique allows a reconstruction of the population distribution of the unperturbed atomic state by observing the rf spectroscopy signal after an abrupt switch-off of the perturbing light. The evolution and relaxation dynamics of the individual magnetic sublevels is investigated. Experimental observations are supported with numerical modeling based on a full density-matrix calculation performed in the presence of spin-exchange collisions and homogeneous relaxation.

DOI: 10.1103/PhysRevA.88.052508 PACS number(s): 32.30.Bv, 32.60.+i, 33.35.+r, 32.70.Jz

## I. INTRODUCTION

Quantum measurements form an important branch of modern metrology. A large variety of frequency standards, magnetometers, and interferometers make use of the quantum properties of nature. Similarly to their classical counterparts, the devices require preparation of a probe (in this case a particular quantum state of atom, photon, or other object), interaction of the probe with a system to be measured, and detection of the probe final state [1]. These three processes are commonly performed during time-separated stages, which are run sequentially. Although conceptually straightforward, the drawback of this approach is a limited access to the information from the system; i.e., the system state can be read out only at specific intervals. In the particular case of frequency standards, it results in dead time that increases the duration of the measurement in order to reach the required stability [2]. Alternatively, the measurements can be performed in a continuous mode, where all three stages occur simultaneously. While this approach avoids dead time, the overlap between the stages may cause a perturbation or even suppression of a weaker process by a more dominant one. Consequently, the outcome of the measurement does not reveal the unperturbed nature of the system. In frequency standards, this may lead to a systematic error or deterioration of the signal-to-noise ratio.

Radio-frequency (rf) spectroscopy is a workhorse for measurements of oscillating magnetic fields as well as a convenient tool for determining the quantum state of an atomic or molecular system [3–5]. The technique is based on the detection of probe light propagating through a medium that is placed in an external dc magnetic field and simultaneously interacts with a strong light beam(s) and a weak rf field. From the quantum measurement perspective the rf spectroscopy consists of three stages: preparation of a state through optical pumping, interaction of the atomic sample with an rf field, and readout of the final state via the weak probe beam. For a linearly polarized probe, the detected signal is rotation of the probe-light polarization; nonzero rotation is observed when the rf-field frequency is tuned to resonance with neighboring magnetic sublevels [6–8]. The signal consists of a resonance or a series of resonances, for which the linewidths are determined by the lifetimes of the coherence between ground-state magnetic sublevels and the amplitudes are proportional to the amplitude of the Zeeman coherences between adjacent sublevels [3]. Thus, monitoring the signal profile provides information about the state of the system and relaxation of the coherence. It should be noted, however, that the simultaneous application of the continuous wave (cw) strong light for optical pumping and an rf field leads to broadening of the resonances and hence distortion of the information about the system state. In particular, this perturbation masks the properties of the dark state [3,5] of interest in many applications [9–11].

The desire to determine the lifetimes of unperturbed quantum states was the main motivation for the development of alternative techniques, in particular the *relaxation in the dark* (RID) technique [12,13]. In the original RID experiment [12], circularly polarized broadband light was used to generate orientation in an atomic ground state. An abrupt block of the light then enabled the system to evolve without any external perturbation, relaxing toward a thermal equilibrium state. Atomic-polarization relaxation was investigated by the detection of the transmitted intensity of light that was switched back on after a variable dark period. The technique allowed observation of longer relaxation times in anti-relaxation-coated and buffer-gas-filled alkali-metal vapor cells and also determined various relaxation cross sections in these systems [12,14].

A modification of the original RID technique relying on magneto-optical rotation of weak probe light was reported in Ref. [15]. In that version of the technique, a cw linearly polarized probe was propagating collinearly with circularly polarized pump light. The atomic-orientation-generating pump was periodically blocked and the rotation of the probe-light polarization was detected. The far-off-resonance detuning of the probe beam ensured that the light did not affect the atomic state in the course of "bright" (pump light on) and "dark" (no pump light) phases. Measurements of the magneto-optical rotation of the probe beam during the no-pump-light period enabled the identification of three distinct relaxation mechanisms responsible for atomic-polarization relaxation: electron-randomization collisions with paraffin-coated cell walls or gaseous impurities, spin-exchange collisions (SECs), and uniform relaxation, e.g., the reservoir effect [15].

 

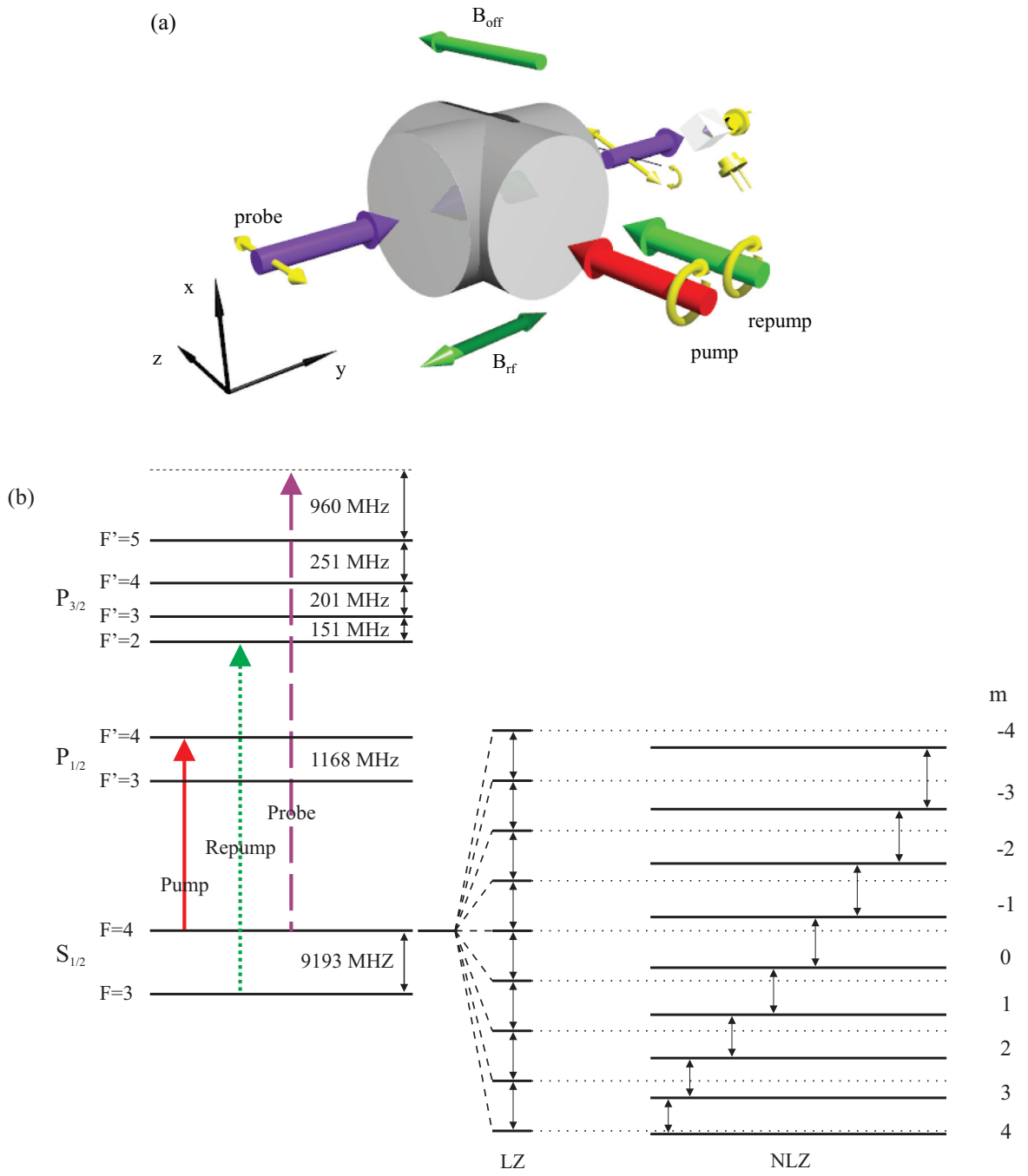


FIG. 1. (Color online) (a) Geometry of the experiment. Two circularly polarized light beams propagating along the $z$ axis optically pump the sample of Cs atoms contained in a paraffin-coated glass cell. A linearly polarized probe beam propagates along the $y$ direction. The polarization of the probe light is parallel to $B_{\text{off}}$ ($z$ direction). The polarization state of the light after traversing the atomic sample is measured with a balanced polarimeter. The oscillating field $B_{\text{rf}}$ oriented orthogonally to $B_{\text{off}}$ creates oscillations of the rotation of the probe light. (b) Cesium $6\,^2S_{1/2} \rightarrow 6\,^2P_{1/2}$ transition ($D_1$ line) and $6\,^2S_{1/2} \rightarrow 6\,^2P_{3/2}$ transition ($D_2$ line) energy structure with the splitting of the $6\,^2S_{1/2}$ $F = 4$ state caused by the linear (LZ) and nonlinear (NLZ) component of the Zeeman effects. The single-ended arrows represent the frequencies of the laser beams used in the experiments (solid red: pump; dotted green: repump; dashed purple: probe), and the double-ended arrows represent the rf transitions between neighboring sublevels.

While RID measurements provide information about unperturbed relaxation times they do not provide detailed information about the atomic population distribution. Traditional rf spectroscopy, on the other hand, is very well suited to deriving information about population distributions. In this paper we describe a technique that modifies rf spectroscopy so as to take advantage of the principles of relaxation in the dark, and call it rf spectroscopy in the dark (SID). The modification consists of an abrupt block of the pump light, and monitoring of the system dynamics through rotation of

the cw off-resonant probe beam polarization (as in RID [15]), in the presence of a weak rf field (as in rf spectroscopy). The rotation signal is demodulated at the rf-field frequency (lock-in). The measurements of the demodulated signals are performed in the presence of a dc magnetic field [Fig. 1(a)]. The magnetic field is strong enough to induce a nonlinear Zeeman (NLZ) splitting of the magnetic sublevels that is larger than the ground-state relaxation rate. This ensures that the applied rf field couples only a single pair of neighboring magnetic sublevels [Fig. 1(b)]. The selectivity of coupling allows an investigation of the relaxation of specific magnetic sublevels and enables their various relaxation dynamics to be determined. The realization of this modified rf spectroscopy is performed in strongly polarized samples (e.g., orientation, as defined in Ref. [3], equal to 0.996). Such systems are of great significance in many areas of atomic physics. In particular, transitions involving a stretched state, i.e., a state with the maximum or minimum $m$, are being used in operation of the chip scale atomic clock [16]. In traditional rf spectroscopy, the strong optical pumping suppresses the rf generation of Zeeman coherences, which consequently leads to a reduction of the rf resonance amplitude(s). Our approach however, facilitates measurements in which the unperturbed amplitudes of the rf transitions are revealed. Apart from the standard measurement of relaxation rates, the implementation of a modified rf spectroscopy enables time-dependent spectroscopy that allows a reconstruction of the population distribution, an extraction of interaction parameters such as the Rabi frequency, as well as demonstrating the different dynamics of magnetic sublevel relaxation. Our experimental observations are supported by calculations including all the key elements of the measurement, i.e., optical pumping, interaction with the rf field, and spin-exchange collisions [17].

## II. EXPERIMENTAL SETUP

A sample of thermal cesium atoms (atomic vapor) is housed in a paraffin-coated, cross-shaped glass cell (22 mm in diameter and arm lengths of 32 mm) [Fig. 1(a)]. The temperature of the vapor is stabilized to within 0.1 °C by temperature-controlled water flowing around the cell. Such stabilization enables precise control over the vapor density and the temperature of the coating, which are two parameters determining relaxation of the atomic state. The ambient magnetic field is suppressed by the use of five layers of cylindrical shields made from 2-mm-thick $\mu$-metal with end caps. Measurements confirmed that the shielding factor of static magnetic fields is better than $3 \times 10^6$. A set of two solenoids inside the shield generates a well-controlled offset magnetic field $B_{\text{off}}$ with a relative homogeneity better than $10^{-5}$ over the length of the cell. A set of ports in the shields provides optical access along and perpendicular to the field $B_{\text{off}}$. The alkali-metal atoms are optically pumped by two circularly polarized laser beams of 20 mm in diameter propagating along the direction of $B_{\text{off}}$. The beams are generated by external cavity diode lasers, frequency locked to the $6\,^2S_{1/2}\ F = 4 \rightarrow 6\,^2P_{1/2}\ F' = 4$ transition of the cesium $D_1$ line (894 nm, pump) and the $6\,^2S_{1/2}\ F = 3 \rightarrow 6\,^2P_{3/2}\ F' = 2$ transition of the cesium $D_2$ line (852 nm, repump) using the Doppler-free dichroic vapor laser lock [18]. The beams are additionally monitored with a standard saturated-absorption setup. Repumping is realized by the recently demonstrated technique of indirect optical pumping [5]. It relies on transferring the orientation created in the F = 3 manifold to the F = 4 manifold through off-resonant optical pumping combined with spin-exchange collisions. A third beam—the probe (2 mm in diameter)—is $z$ polarized and propagates along the $y$ axis, i.e., orthogonally to the offset magnetic field. The polarization of the probe beam is set by a zero-order wave plate and a Glan-Taylor polarizer (extinction better than $10^{-5}$). The probe light is provided by a diode laser operating on the cesium $D_2$ line and frequency stabilized to the $6\,^2S_{1/2}\ F = 4 \rightarrow 6\,^2P_{3/2}\ F' = 5$ transition using a standard saturated-absorption setup. The light is 960 MHz frequency shifted to the blue by two acousto-optic modulators operating in double-pass configuration. An rf field oscillating along the $y$ direction is created by a set of transverse coils. The probe light transmitted through the cell is analyzed by a polarimeter consisting of a crystal polarizer oriented at 45° with respect to the incident polarization and commercial balanced photodetectors. The resulting signal is measured at the first harmonic of the rf-field frequency by a lock-in amplifier.

## III. THEORETICAL MODELING

To theoretically investigate the system under consideration, time-dependent density-matrix calculations are performed. In this paper, we only introduce the key elements of the calculations; a complete description of the calculations will be presented elsewhere [17].

The atomic structure of cesium is modeled by a four-level system with two ground states with $F = 3$ and $F = 4$ and two excited states with $F' = 4$ and $F' = 5$ (practical limitations such as the matrix complexity and the time of the computations restrict the number of levels considered in modeling). The two ground states are coupled to the $F' = 4$ excited state with two strong, circularly polarized light beams ($\Delta m = -1$, where $m$ is the magnetic quantum number and the quantization axis is oriented along $z$). In the simulations, we introduce an external condition that no coherence between the sublevels of the two ground-state hyperfine levels may be generated. It corresponds well to the experimental conditions, where each of the ground states is coupled to a different excited state. It was verified that this approach reproduces results (amplitudes, widths, number of resonances, etc.) obtained in a system, where the pump light couples the ground state with the $F' = 2$ excited state. Weak linearly polarized probe light is tuned 1 GHz into the blue from the $F = 4 \rightarrow F' = 5$ transition and the polarization rotation of this beam is calculated. The degeneracy of the Zeeman sublevels within a given state is lifted by the application of a longitudinal magnetic field. To model realistically the conditions of the experiment, the Zeeman interaction includes nonlinear terms, as well as the nuclear contribution to the respective Landé factors. The atoms additionally interact with a weak oscillating magnetic field coupling Zeeman sublevels within a given state. For simplicity of the simulations, the nonresonant rf coupling of the excited state, which has a much smaller influence on the system due to the small occupation of the excited states and much larger relaxation rates of those states, has not been shown in the diagram. The system used for simulations is shown in Fig. 2.

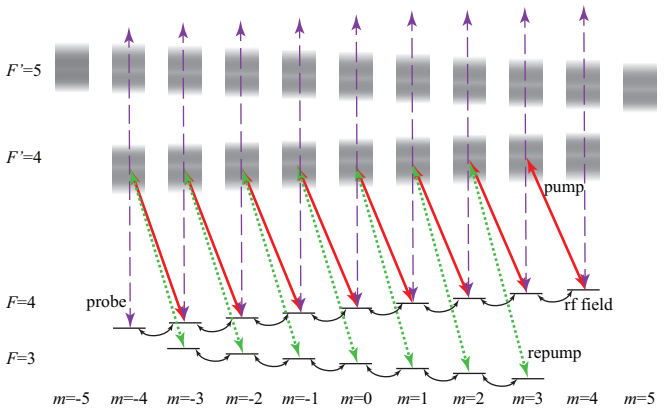


FIG. 2. (Color online) Energy-level diagram of the model system used for density-matrix calculations. The red (solid) and green (dotted) arrows correspond to the strong pump and repump beams, respectively, and the dashed purple arrows denote the weak probe light. Small black arrows connecting neighboring Zeeman sublevels correspond to rf-field coupling.

The model developed considers two types of relaxation—homogeneous (uniform) and inhomogeneous relaxation. The first type of relaxation is induced by all processes that are independent of the particular quantum state of the relaxing atoms. A specific example of homogeneous relaxation is collisions of polarized atoms with uncoated surfaces, in which the information about the initial state of the atom is completely lost. Inhomogeneous relaxation is induced by all processes that are sensitive to the initial state of the relaxing atom. One example is spontaneous emission in which selection rules of optical transitions need to be fulfilled. Another example is spin-exchange collisions [19], in which the total angular momentum of the colliding object is conserved and the system evolves toward an equilibrium state with a spin-temperature-population distribution [20]. As shown in Ref. [5], this relaxation mechanism allows the generation of high atomic polarization without any power broadening. Yet, as shown in this paper, even in this power-broadening-free arrangement, the amplitudes of the observed rf resonances are slightly decreased with respect to the completely unperturbed optical system.

The evolution of the density matrix $\rho$ is calculated based on the Liouville equation,

$$\dot{\rho} = -\frac{i}{\hbar}[H,\rho] - \Gamma(\rho), \tag{1}$$

where $H$ is the full Hamiltonian of the system including optical excitations and interaction with static and oscillating magnetic fields, and $\Gamma(\rho)$ is the operator responsible for all the different types of relaxation. It can be shown [17] that the angle $\varphi$ of magneto-optical rotation of the $z$-polarized probe light propagating along $y$, where $z$ is the quantization axis, is

$$\varphi \propto \sum_{j=-F}^{F-1} \langle Fj+110|F'j+1\rangle \rho_{Fj,F'j+1} - \sum_{j=-F+1}^{F} \langle Fj-110|F'j-1\rangle \rho_{Fj,F'j-1}, \tag{2}$$

where $\rho_{Fj,F'j'}$ is the time-dependent density-matrix element between the $|Fj\rangle$ and $|F'j'\rangle$ states and $\langle\,|\,\rangle$ denotes the Clebsch-Gordan coefficient. In order to calculate the amplitude of the probe rotation due to the rf field, i.e., the signal detected experimentally, the time-dependent rotation given by Eq. (2) needs to be averaged over a period of the rf field,

$$\varphi_{\text{in}} = \frac{\omega_{\text{rf}}}{\pi}\int_0^{2\pi/\omega_{\text{rf}}} \varphi \sin\omega_{\text{rf}} t\,dt, \qquad \varphi_{\text{quad}} = \frac{\omega_{\text{rf}}}{\pi}\int_0^{2\pi/\omega_{\text{rf}}} \varphi \cos\omega_{\text{rf}} t\,dt, \tag{3}$$

where $\omega_{\text{rf}}$ is the rf-field frequency. The simulation parameters were determined based on independent measurements.

## IV. RESULTS AND DISCUSSION

The results are grouped in five main subsections. The first part discusses standard rf spectroscopy and in particular its limitations as a tool for characterizing strongly perturbed atomic systems. The subsequent subsection introduces briefly the modified rf spectroscopy technique, while the final three parts present and discuss the parameters measured with the technique.

### A. Highly oriented atomic system

Cesium atoms are optically pumped into the $|F=4, m=-4\rangle$ state by two (pump and repump) circularly polarized laser beams [Fig. 1(a)]. The rf spectra can be used to quantify the efficiency of the optical pumping process. Figure 3 shows typical polarization-rotation signals measured as a function of the rf-field frequency for three distinct pump powers (all light beams are on during the measurements). Polarization-rotation resonances are observed when the rf field induces transitions between neighboring magnetic sublevels. Since the position of the resonance is determined by the energy difference between the sublevels, at higher-magnetic fields, where NLZ effects lift the degeneracy, a series of resonances is observed. The amplitude of the resonances depends on the strength of the Zeeman coherence between adjacent sublevels, and to first order, is determined by the population difference between the sublevels [17]. As shown in Fig. 3(a), even for a weak pump (<0.2 $\mu$W), a relatively high orientation of the medium may be generated when the repump beam is intense (200 $\mu$W) [Fig. 3(a)]. This polarization is mainly induced by indirect optical pumping with the repump supported by spin-exchange collisions (for more details see Ref. [5]). At higher pump powers, the polarization of the medium increases, which manifests itself as a deterioration of all resonances except the one corresponding to the $m=-4 \leftrightarrow m=-3$ transition (rightmost resonance) [Fig. 3(b)]. For even higher powers, the resonance broadens and its amplitude decreases [Fig. 3(c)]. This behavior is more apparent in Fig. 4, which shows the systematic observation of pump-power-induced changes of the amplitude [Fig. 4(a)] and width [Fig. 4(b)] of the leading (largest) resonance corresponding to the $m=-3 \leftrightarrow m=-4$ transition. The amplitude and width were extracted by fitting the spectra with a series of Lorentz curves. The three pump powers discussed are representative of three different regimes

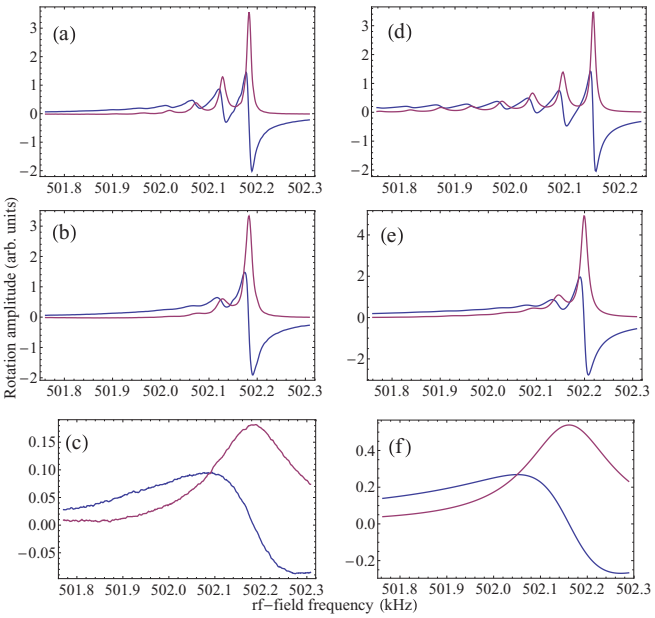


FIG. 3. (Color online) Experimental (a)–(c) and simulated (d)–(f) magneto-optical-rotation signals recorded as a function of the rf-field frequency for three distinct pump-light powers and fixed repump power. Blue (dark gray) curves correpond to the in-phase component ($\varphi_{\text{in}}$), while purple (light gray) ones correspond to the quadrature ($\varphi_{\text{quad}}$) component of the signal. The experimental signals were measured for 0.18 $\mu$W (a), 6.9 $\mu$W (b), and 220 $\mu$W (c) of the pump and 200 $\mu$W of the repump beam. The simulations were performed with pump Rabi frequencies of 10 kHz (d), 40 kHz (e), and 250 kHz (f), and a repump Rabi frequency of 1 MHz. To achieve better qualitative agreement between experimental signals and simulated data, the ratio of the Rabi frequencies of the pump and repump beams has been modified with respect to the experimental conditions (see text).

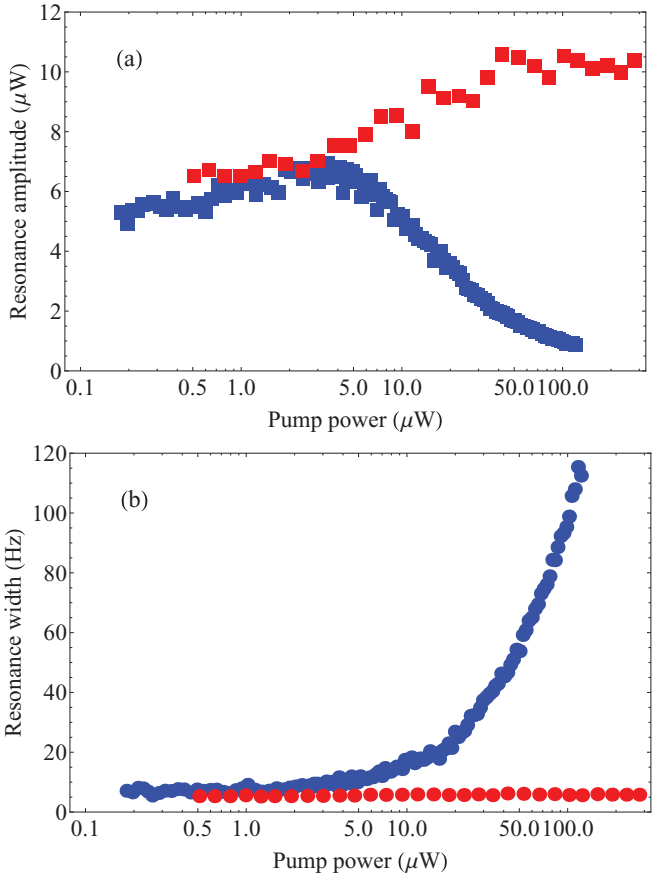


FIG. 4. (Color online) Amplitude (a) and width (b) of the leading resonance in the rf signal (the $m = -4 \leftrightarrow m = -3$ transition) as a function of the pump-beam power with fixed repump-beam power of 200 $\mu$W. In the case of traditional rf spectroscopy, i.e., with both beams on, the parameters of the leading resonance [blue (dark gray) symbols] were obtained by fitting the spectrum with a sum of eight Lorentz curves. The same parameters in the second case [red (light gray) symbols] were extracted from the SID signals according to the procedure described below.

corresponding to (1) constant width and slow increase of the resonance amplitude (pump power $<2$ $\mu$W), (2) broadening of the resonance still with increasing amplitude, and (3) strong broadening of the resonance and deterioration of its amplitude (pump power $>10$ $\mu$W).

The reduction of the signal amplitude can be understood using Bloch-vector terminology [21]. Here, the vertical component of the vector corresponds to the difference in population of the $m = -3$ and $m = -4$ sublevels, the poles of the sphere correspond to population in only one of the sublevels, and the horizontal component of the vector represents the coherences between them [22]. Optical pumping builds up population in the stretched state and thus aligns the Bloch vector in the vertical direction. The rf field interacting with the atomic population generates a coherence that corresponds to the rotation of the Bloch vector towards the horizontal plane. When the strength of the optical interaction dominates over the rf coupling, the Bloch vector is kept in the vertical direction, effectively suppressing the generation of coherences and subsequently reducing the amplitude of the rf resonance [Eq. (2)]; the rf field cannot efficiently generate a coherence in this case because as soon as it couples population into $m = -3$ the atom is excited and hence the coherence is destroyed. In our experimental conditions, this regime is achieved for pump powers above 4 $\mu$W, when the pump Rabi frequency $\Omega_{\text{pump}}$ significantly exceeds the rf Rabi frequency ($\Omega_{\text{rf}} < 1$ Hz for $B_{\text{rf}} = 0.1$ nT).

Figures 3(d)–3(f) present results of numerical simulations for three sets of parameters corresponding to the three regimes. As shown, the obtained shapes agree well with the experimental signals. It should be noted, however, that the agreement was not achieved for parameters extracted from the experiment. It is believed that this discrepency is a consquence of simplifications in our calculations and the presence of additional mechanisms that were not included in our model. In particular, we do not take into account atomic motion and the fact that atoms spend most of their evolution outside the light beam, where they only interact with the magnetic and rf fields. Thus, in contrast to the real situation, in our model, there is a continuous competition between optical and rf interactions. This difference manifests as systematically lower values of the Rabi frequencies used for the simulations than those observed in our experiment (in the experiment, the atoms experience an effective Rabi frequency,

i.e., a Rabi frequency that is averaged over the cell volume). Interestingly, the difference is larger for lower light powers than for higher powers. We attribute this to more complex excited-level structure of the real system than used in the simulation and off-resonance excitation of the levels, which enhance the pumping efficiency.

The presented spectra show that application of intense cw pump light strongly perturbs the system and modifies the observed rf spectra. A decrease of the amplitude of individual resonances, accompanied by their broadening, complicates analysis of the signals, making fitting of the recorded spectra particulary hard. As a result, a reconstruction of the atomic-population distribution is more challenging or may even be completely impossible. In particular, in the rf spectrum shown in Fig. 3(c), the amplitude of the line corresponding to $m = -3 \leftrightarrow m = -4$ transition is ten times larger than that corresponding to $m = -2 \leftrightarrow m = -3$, and 100 times bigger than the $m = -1 \leftrightarrow m = -2$ transition even though the population differences between the sublevels may not be in the corresponding ratios [23]. This clearly implies the necessity to develop a technique that enables extraction of information about the system and its relaxation dynamics even under such strongly perturbing experimental conditions.

### B. Rf spectroscopy in the dark

In order to perform a reconstruction of the unperturbed population distribution and obtain information about some of the system parameters, a modified version of rf spectroscopy is used. The pump and repump beams are switched off, leaving the initially polarized system to evolve in the presence of the probe beam (as in RID measurement [15]) and a weak perturbation from the rf field. The presence of the rf field enables the evolution of selected magnetic sublevels to be investigated. Thus, in the current configuration where the rotation signal is demodulated at the rf-field frequency (lock-in detection), the probe beam monitors ground-state coherences and their relaxation [24]. With no optical pumping the ground-state coherences can be efficently created by the rf field, and the resonant amplitude of the polarization-rotation signal is determined simply by the population difference between them and is not supressed by the pump.

To stress the difference between the current approach and the one described in Ref. [15], two features of our technique need to be pointed out. First, in our arrangement, the rotation signal is determined by the coherence between rf-field coupled Zeeman sublevels and not by the population ditribution among the sublevels (as in traditional RID). Thus, the method does not provide direct information about the polarization of the atoms but more complete information about their quantum states, i.e., Zeeman coherences and, indirectly, population of the sublevels. The consequence of observing the signals determined by the coherences, and thus the second difference between SID and RID, is the ability to investigate the transverse relaxation time ($T_2$) rather than the longitudinal relaxation time ($T_1$) [15]. In general, these two relaxations may be determined by different processes, i.e., additional dephasing may be present in the system. For example, SECs preserve the total angular momentum of the colliding atoms; thus they do not lead (to the first order) to deterioration of the traditional RID signal (see Eq. (8) in Ref. [15]), while here SECs are partially responsible for the decrease of the signal ampitude. Additionally, the dependence of the transverse relaxation on the magnetic field is theoretically predicted [20,25], but there is no similar dependence for the longitudinal relaxation. Knowledge about the quantum state of atoms and the dynamics of their relaxation is important for quantum-state engineering and quantum-information processing, as well as atomic magnetometry.

### C. Interaction with rf field and Rabi flopping

Figure 5(a) shows typical quadrature components of the signals measured in our SID arrangement. The two presented cases correspond to measurements with the rf field tuned to the center of the $m = -4 \leftrightarrow m = -3$ transition and detuned several linewidths from the center [Fig. 5(a)]. At $t = 0$, the pumping beams (pump and repump) are switched off and the system starts to evolve toward thermal equilibrium. When the rf field is tuned in the vicinity of the resonance center [blue (dark gray) curve], a strong initial increase of polarization-rotation amplitude is observed. This arises from the rf-field-induced buildup of the coherence. The amount of the rotation increase depends on the pump-beam power, i.e., the transverse relaxation the light had introduced. After this initial enhancement, a deterioration of the signal amplitude is observed. The signal behavior is different when the frequency of the rf field is detuned several linewidths from the resonance

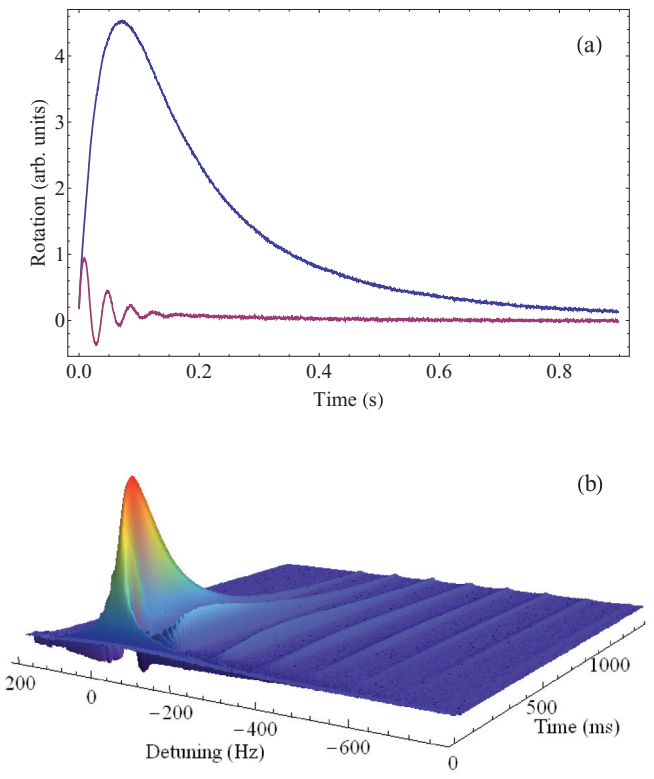


FIG. 5. (Color online) (a) Temporal dependence of the experimentally measured magneto-optical-rotation signal after switching off a strong pump beam (100 $\mu$W) at $t = 0$. The blue (dark gray) curve shows the rf field on resonance, while the purple (light gray) curve is for a 26 Hz detuning. (b) Experimental dependence of the SID signal on frequency of rf-field tuning.

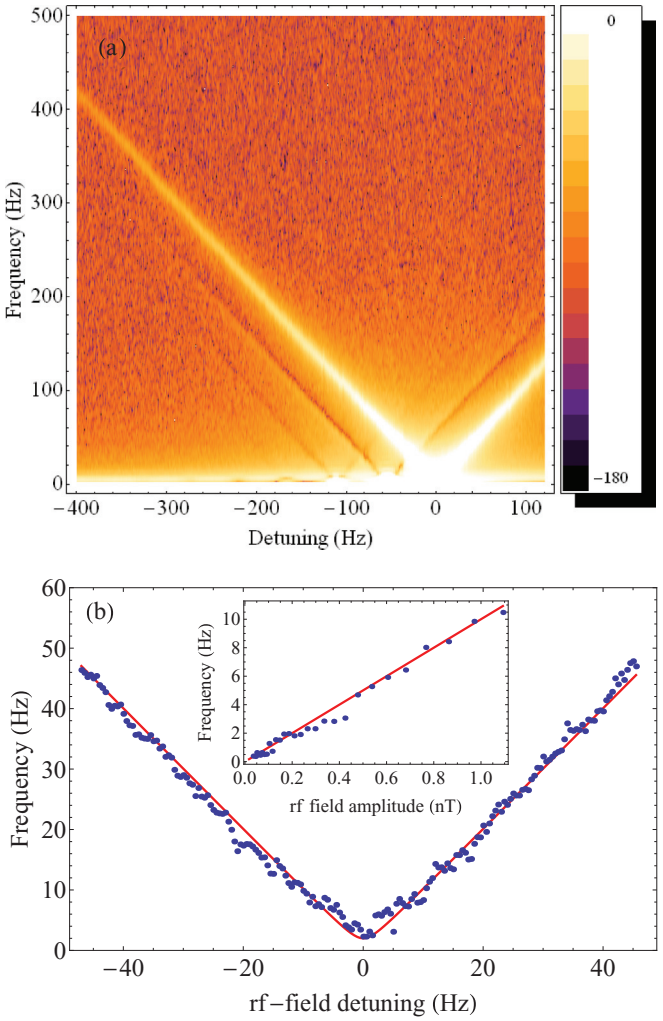


FIG. 6. (Color online) (a) Dependence of the power spectral density of the Fourier transform components, corresponding to Rabi oscillations (measured just after turning off the light) on the rf-field frequency with a pump laser power of ∼200 $\mu$W; $\Omega_{rf}/2\pi = 0.2$ Hz. (b) Frequency of the signal oscillations as a function of the detunings of the rf field from the $m = -4 \leftrightarrow m = -3$ transition [red (light gray) curve Rabi frequency formula; $\Omega_{rf}/2\pi = 2$ Hz]. Inset presents the dependence of the frequency of the oscillations at the resonance on the amplitude of the rf field.

[purple (light gray) curve]. In that case, the oscillations of the signal are observed but their amplitude is significantly smaller than the maximum rotation detected in the on-resonance case. It was observed that the amplitude of the oscillations diminishes with the detuning, while their frequency increases with the detuning. This suggests that the oscillations arise due to the Rabi flopping of populations between two states coupled by the rf field.

To confirm that the observed oscillations are indeed due to Rabi flopping, a series of SID signals for different rf-field tunings was measured [Fig. 5(b)]. The map reveals a number of resonances corresponding to transitions between sucessive sublevels. The amplitudes of the individual resonances reflect the amplitudes of the coherences between the given pair of sublevels and hence the population difference between them.

Figure 6(a) shows a power-spectral-density (psd) map of the signal shown in Fig. 5(b). The map reveals a number of traces associated with different rf resonances corresponding to the $m = -4 \leftrightarrow m = -3$, $m = -3 \leftrightarrow m = -2$, and $m = -2 \leftrightarrow m = -1$ transitions. Each of them has a trace consisting of two symmetric branches, which depend linearly on the detuning. This dependence is as expected from the generalized Rabi frequency $\tilde{\Omega}_{rf} = \sqrt{\delta_{rf}^2 + \Omega_{rf}^2}$, which for larger detunings, $\delta_{rf}/\Omega_{rf} \gg 1$ takes the form $\tilde{\Omega}_{rf} \approx |\delta_{rf}|$ ($\delta_{rf}$ is the detuning and $\Omega_{rf}$ is the on-resonance Rabi frequency). Interestingly, all the traces except the one corresponding to the strongest transition are negative (dark shades with respect to the background). This behavior is a signature of the beating between various transitions and negative interference between the Fourier components [26].

While the map shown in Fig. 6(a) gives qualitative information about the effect, it has its limitations; since the signals are not periodic, some artificial features may also be present in their Fourier spectra. Thus, in order to obtain quantitative information about the rf-field Rabi frequency, the time-dependent SID signal for the $m = -4 \leftrightarrow m = -3$ resonance [Fig. 5(b)] was fitted with an analytical formula,

$$\phi_{quad} = \alpha_1 e^{-\gamma_1 t} + \alpha_2 e^{-\gamma_2 t} \sin(\omega t), \tag{4}$$

where $\alpha_1$ is the amplitude of the static component of the signal, $\alpha_2$ is the amplitude of the oscillation, $\gamma_1$ and $\gamma_2$ are the corresponding relaxation rates, and $\omega$ is the frequency of the oscillations [27]. The fitting confirmed that the signal oscillations occur at the generalized Rabi frequency, i.e., the signal-oscillation frequency $\omega$ scales with the detuning according to the formula given above for $\tilde{\Omega}_{rf}$ [Fig. 6(b)]. Moreover, since the amplitude of the rf field used in most measurements is relatively low and the frequency of the oscillations far from the resonance is equal to the detuning, we were able to determine the on-resonance rf-field Rabi frequency $\Omega_{rf}$ ($\Omega_{rf}/2\pi = 2$ Hz) and demonstrate that it scales linearly with the amplitude of the field [inset in Fig. 6(b)]. The ability to determine the Rabi frequency enables a direct measurement of the coupling strength between the rf field and the atoms, which in turn enables a determination of the magnetic-field strength. This is important not only for magnetometry but also for coherent manipulation of the quantum state of a system. For example, knowledge about the coupling strength allows various operations to be performed on qubits.

### D. Population distribution

The dependence of the oscillation amplitude $\alpha_2$ on the rf-field frequency reveals the unperturbed profile of an rf resonance, i.e., its amplitude, width, and central frequency. Figure 7 shows the profile of the strongest resonance [purple (light gray) curve] extracted from the fittings [Eq. (4)] to the signal at various rf-field detunings (dependence of $\alpha_2$ on $\delta_{rf}$). The extracted width is about 5.5 Hz and is roughly 30 times smaller than the width measured with both light beams on [blue (dark gray) curve]. Additionally, a 5-Hz shift between the two curves is observed. This is introduced by the ac Stark shift due to the pump and/or repump beams.

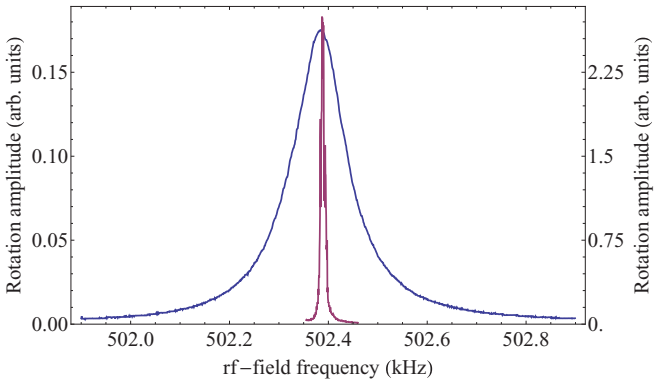


FIG. 7. (Color online) Rf spectrum of polarization rotation in the presence of pump and repump beams [blue (dark gray)] and the resonance profile extracted from the SID signals after the beams were blocked [purple (light gray)]. The amplitude of the resonance from SID signals is about 15 times larger (right scale) than that measured directly using rf spectrum (left scale).

Using SID measurements and the fitting procedure decribed above, the amplitude and width dependence of the signal on pump power was measured (Fig. 4). As shown, the width [red (light gray) circles] is independent of the pump (and repump) powers while the amplitude [red (light gray) squares] rises with the power until it saturates. This saturation corresponds to complete polarization of the medium (experimentally detected population of $m = -4$ level of 98.6%, 1.2% in $m = -3$, 0.2% in $m = -2$ were measured at $t>0$ and may be extrapolated to $t = 0$) [3,5]. It is imporant to stress that these populations were extracted from the system, which, under the conditions of rf spectroscopy, corresponds to the signal shown in Fig. 3(c). The ability to determine the populations of the magnetic sublevels of a strongly polarized system is an important advantage of our SID technique over the traditional rf spectroscopy. This may be shown by the example of quantum-information experiments exploiting continuous-variable systems such as thermal atomic ensembles [28]. Implementation of various entanglement and quantum-communication protocols utilizes atoms in highly polarized states (known also as the coherent spin states). These highly polarized states are typically obtained by optical pumping of atoms with intense light, which strongly perturbs the system, masking some of its characteristics. In particular, power broadening of the resonances prevents precise determination of the amplitudes and widths of the observed signals. Yet, "for fault-tolerant quantum computing initialization fidelities exceeding 0.9999 are desirable" [29]. As pointed out in Ref. [3], traditionally "it takes some effort and experimental stability to see the difference between a 98% and a 100% polarized sample." With our technique, such a level of precision is easily accessible.

### E. Rf spectroscopy in the dark and spin-exchange collisions

Figure 8(a) shows the dependence of the SID signal for highly polarized samples with an rf field tuned to successive $m =\leftrightarrow m = +1$ transitions of the $F = 4$ state. The initial flat part of the signal (up to 0 ms) corresponds to the case of strong optical pumping (both light beams on). During this time the largest rf resonance corresponding to the $m = -4 \leftrightarrow m = -3$ transition is roughly ten times larger than the second largest resonance (the $m = -3 \leftrightarrow m = -2$ transition) [23]. At $t = 0$ the light beams are switched off and the system starts to relax. First, enhancement of the rotation is observed. As discussed above, the enhancement is due to the generation of Zeeman coherence with the rf field. Interestingly, larger (relative) enhancements are observed when the rf field is tuned to transitions other than the $m = -4 \leftrightarrow m = -3$ transition. This originates from the fact that for $t<0$, there is almost no population in any of the states except for the $|F = 4, m = -4\rangle$ state. When the system relaxes, the other sublevels ($m> -4$) are being repopulated and the coherence between them can be established. It is crucial in this context to note that different dynamics are involved in the repopulation of the sublevels. This manifests itself in the appearance of the maximum SID signal at different $t$ for different rf transitions and originates from the coexistence of two relaxation processes in the system. While uniform relaxation acts to equalize the population among the sublevels, SEC relaxation acts to generate a spin-temperature-population distribution [20,25]. This was verified

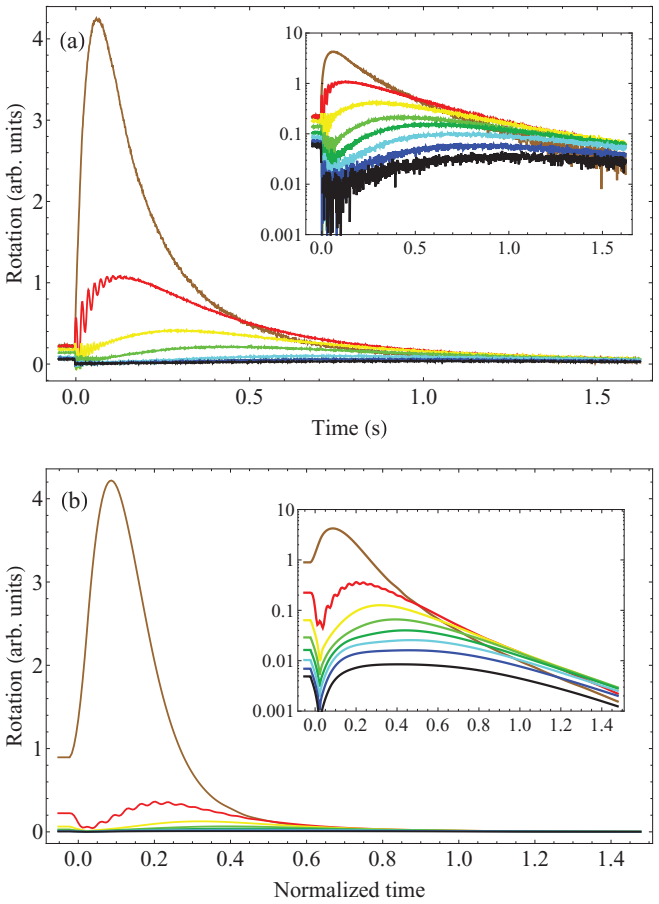


FIG. 8. (Color online) SID signals observed experimentally (a) and simulated numerically (b) for the rf field tuned to a given $m =\leftrightarrow m = +1$ transition (insets present SID signals in logarithmic scale). The experimental signals were measured for a highly polarized sample (98.6% of population in $m = -4$) for 200-$\mu$W pump-beam and 200-$\mu$W repump-beam powers, while the simulations were performed with ($\Omega_{\text{pump}}/2\pi = 250$ kHz, $\Omega_{\text{repump}}/2\pi = 1$ MHz). Both simulations and measurements were performed with $\Omega_{\text{Larmor}}/2\pi =$ 502 kHz corresponding to a nonlinear Zeeman splitting of ∼50 Hz.

by numerical simulations based on the rate-equation model that this competition leads to temporal differences in buildup of population of the sublevels, and hence various dynamics of the SID signals. Monitoring of the dynamics of various coherences (populations) is only possible through the presence of the rf field that generates coherences during the dark phase and would not be possible using other existing techniques (such as RID).

Figure 8(b) shows the numerical simulations performed for a highly polarized sample (full density-matrix simulations). The simulations reveal the same features as measured experimentally, i.e., the initial constant signal with both beams on, the different times the signals maximize, and the oscillations due to off-resonant coupling to the $m = -4 \leftrightarrow m = -3$ transition. Using simulations we were able to show that the sublevel repopulation is responsible for the different dynamics of the SID signals corresponding to the particular transitions. Although the simulations predict all the qualitative features of the signal, quantitatively there is not such a good agreement, which once again originates from simplifications of our model.

## V. CONCLUSIONS

In this paper, we have demonstrated a modified rf spectroscopy technique, which, owing to the application of an rf field, allows an investigation of the dynamics of coherence generation and population redistribution. Using the technique we present a reconstruction of the atomic population distribution in a highly oriented atomic sample. Systems with a high level of orientation are of great importance in atomic magnetometry [7,10], frequency standards [16], and quantum-information processing [30]. Accurate diagnostic tools could aid further development of a precise sensor based on these systems. Since a reconstruction is not possible in traditional experiments when strong cw light is used, modified rf spectroscopy may be attractive for quantum-state tomography. In particular, we have demonstrated a determination of the population distribution (98.6% in $m = -4$, 1.2% in $m = -3$, 0.2% in $m = -2$ sublevel) and an extraction of interaction parameters such as the rf-field Rabi frequency. Finally, it was shown that the technique enables the relaxation dynamics of specific magnetic sublevels to be investigated, which allowed us to demonstrate that the repopulation of magnetic sublevels in a polarized sample depends on $m$.

## ACKNOWLEDGMENTS

The work was funded by the UK NMS Programme and the National Centre for Research and Development with the Leader Programme. The authors would like to acknowledge D. Budker and B. Patton for stimulating discussion.

[1] V. B. Braginsky and F. Ya. Khalili, *Quantum Measurement* (Cambridge University Press, Cambridge, 1992).
[2] R. Wynands and S. Weyers, Metrologia **42**, 64 (2005).
[3] B. Julsgaard, J. Sherson, J. L. Sørensen, and E. S. Polzik, J. Opt. B: Quantum Semiclass. Opt. **6**, 5 (2004).
[4] B. Wang, Y. Han, J. Xiao, X. Yang, C. Zhang, H. Wang, M. Xiao, and K. Peng, Phys. Rev. A **75**, 051801 (2007).
[5] W. Chalupczak, R. M. Godun, P. Anielski, A. Wojciechowski, S. Pustelny, and W. Gawlik, Phys. Rev. A **85**, 043402 (2012).
[6] E. B. Aleksandrov and M. V. Balabas, Opt. Spectrosc. **69**, 4 (1990); S. Groeger, G. Bison, J.-L. Schenker, R. Wynands, and A. Weis, Eur. Phys. J. D **38**, 239 (2006).
[7] M. P. Ledbetter, I. M. Savukov, V. M. Acosta, D. Budker, and M. V. Romalis, Phys. Rev. A **77**, 033408 (2008).
[8] A. Weis, G. Bison, and A. S. Pazgalev, Phys. Rev. A **74**, 033401 (2006); G. Di Domenico, G. Bison, S. Groeger, P. Knowles, A. S. Pazgalev, M. Rebetez, H. Saudan, and A. Weis, *ibid.* **74**, 063415 (2006); G. Di Domenico, H. Saudan, G. Bison, P. Knowles, and A. Weis, *ibid.* **76**, 023407 (2007).
[9] W. Chalupczak, R. M. Godun, S. Pustelny, and W. Gawlik, Appl. Phys. Lett. **100**, 242401 (2012).
[10] I. M. Savukov, S. J. Seltzer, M. V. Romalis, and K. L. Sauer, Phys. Rev. Lett. **95**, 063004 (2005).
[11] W. Wasilewski, K. Jensen, H. Krauter, J. J. Renema, M. V. Balabas, and E. S. Polzik, Phys. Rev. Lett. **104**, 133601 (2010).
[12] W. Franzen and A. G. Emslie, Phys. Rev. **108**, 1453 (1957).
[13] W. Franzen, Phys. Rev. **115**, 850 (1959); H. G. Dehmelt, *ibid.* **105**, 1487 (1957).
[14] L. W. Anderson and A. T. Ramsey, Phys. Rev. **124**, 1862 (1961); F. A. Franz and E. Luscher, *ibid.* **135**, A582 (1964).
[15] M. T. Graf, D. F. Kimball, S. M. Rochester, K. Kerner, C. Wong, D. Budker, E. B. Alexandrov, M. V. Balabas, and V. V. Yashchuk, Phys. Rev. A **72**, 023401 (2005).
[16] Y.-Y. Jau *et al.*, Phys. Rev. Lett. **92**, 110801 (2004).
[17] S. Pustelny and W. Chalupczak (unpublished).
[18] G. Wasik, W. Gawlik, J. Zachorowski, and W. Zawadzki, Appl. Phys. B **75**, 613 (2002).
[19] W. Happer, Rev. Mod. Phys. **44**, 169 (1972).
[20] D. K. Walter and W. Happer, Laser Phys. **12**, 1182 (2002).
[21] L. Allen and J. H. Eberly, *Optical Resonance and Two-Level Atoms* (John Wiley and Sons, Chichester, UK, 1975).
[22] Equivalent description could be done in terms of collective total angular momentum, e.g., [11].
[23] This observation is based on systematic measurements of the amplitudes of all rf resonances versus the pump power (for better clarity, only the amplitude of the signal of the $m = -4 \leftrightarrow m = -3$ resonance is shown in Fig. 4).
[24] Systematic studies confirm that the probe-light influence may be neglected due to its off-resonance detuning (in other words neither deviation from linear resonance amplitude dependence on probe power nor change in resonance width due to probe beam presence is observed within probe laser power range used in SID measurements).
[25] S. Appelt, A. B.-A. Baranga, C. J. Erickson, M. V. Romalis, A. R. Young, and W. Happer, Phys. Rev. A **58**, 1412 (1998).

[26] Because of the beating between different components of the signal the sign of the traces corresponding to the weaker transitions depends on the measurement moment.

[27] We use phenomenological formula that takes into account temporal change of the relaxation rate. This results from the modifications in atomic population distributions [5]. For instance, in highly polarized samples, the relaxation associated with SECs is suppressed [e.g., S. Appelt, A. B.-A. Baranga, A. R. Young, and W. Happer, Phys. Rev. A **59**, 2078 (1999)]. So for small $t$ the atoms relax mainly due to uniform relaxation. The process slowly repopulates the sublevels, simultaneously turning on the SEC relaxation.

[28] N. J. Cerf, G. Leuchs, and E. S. Polzik, *Quantum Information with Continuous Variables of Atoms and Light* (Imperial College Press, London, 2007).

[29] H. Häffner, C. F. Roos, and R. Blatt, Phys. Rep. **469**, 155 (2008).

[30] J. F. Sherson, H. Krauter, R. K. Olsson, B. Julsgaard, K. Hammerer, I. Cirac, and E. S. Polzik, Nature **443**, 557 (2006).